

Many-body effects in suspended graphene probed through magneto-phonon resonances

Stéphane Berciaud,^{1,2,*} Marek Potemski,³ and Clément Faugeras^{3,†}

¹*Université de Strasbourg, CNRS, Institut de Physique et Chimie des Matériaux de Strasbourg, UMR 7504, F-67000 Strasbourg, France*

²*Institut Universitaire de France, 1 rue Descartes, 75231 Paris cedex 05, France*

³*Laboratoire National des Champs Magnétiques Intenses, CNRS/UJF/UPS/INSA, Grenoble F-38042, France*

We make use of micro-magneto Raman scattering spectroscopy to probe magneto-phonon resonances (MPR) in suspended mono- to penta-layer graphene. MPR correspond to avoided crossings between zone-center optical phonons (G-mode) and optically-active inter Landau level (LL) transitions and provide a tool to perform LL spectroscopy at a fixed energy (≈ 197 meV) set by the G-mode phonon. Using a single-particle effective bilayer model, we readily extract the velocity parameter associated with each MPR. A single velocity parameter slightly above the bulk graphite value suffices to fit all MPR for $N \geq 2$ layer systems. In contrast, in monolayer graphene, we find that the velocity parameter increases significantly from $(1.23 \pm 0.01) \times 10^6$ m.s⁻¹ up to $(1.45 \pm 0.02) \times 10^6$ m.s⁻¹ as the first to third optically-active inter LL transition couple to the G-mode phonon. This result is understood as a signature of enhanced many-body effects in unscreened graphene.

Pristine suspended monolayer graphene is a well-defined, unscreened two-dimensional electronic system, in which a wealth of intriguing electronic [1–5], optical [6] and mechanical [7] properties have been uncovered. In particular, spectacular deviations from a simple one-electron picture of graphene’s band structure (i.e., the Dirac cones) emerge at low carrier densities (below a few 10^{11} cm⁻²). Due to electron-electron interactions, the velocity parameter diverges logarithmically as the Fermi energy approaches the Dirac point [4], reaching values, well above the Fermi velocities of bulk graphite and supported graphene ($\sim 1 \times 10^6$ m.s⁻¹) [8].

In the presence of a transverse magnetic field B , the electronic states of graphene merge into discrete, highly degenerate Landau Levels (LL) [9]. The energy and lifetime of LL can be probed using magneto-transport measurements [1, 4], scanning tunnelling spectroscopy [10] and magneto-optical spectroscopies [9, 11]. Recently, micro-magneto-Raman spectroscopy (MMRS) [12–17] has been employed to probe the electronic dispersion of suspended graphene layers [14] and also to demonstrate that electronic excitations between LL may be strongly affected by many-body effects. First, as B decreases, the energy of a given LL also decreases and electron-electron interactions lead to a logarithmic divergence of the corresponding velocity parameter (hereafter denoted v_F for simplicity) [5, 16, 18]. Second, inter LL excitations lead to the formation of magneto-excitons, whose binding energies depend on the index n of the electron and hole LL they arise from, leading to n -dependent v_F [5].

Thus far, Raman signatures of many-body effects have predominantly appeared on the electronic Raman scattering response of graphene [19] under a transverse magnetic field [5, 14]. Recently, many-body effects have also been unveiled by monitoring magneto-phonon resonances [12] (MPR) between optically-active inter-LL

transitions [20] and zone-center optical phonons (i.e., Raman G-mode phonons [21]) in graphene encapsulated in hexagonal boron nitride (BN) films [16]. As recently suggested by Sonntag *et al.* [18], more prominent effects are expected in suspended graphene, where electron-electron interactions are minimally screened.

In this letter, we report the results of MMRS measurements performed on suspended mono- to pentalayer graphene. For each number of layers N , we resolve a set of well-defined MPR. Using a single-particle effective bilayer model, we readily extract v_F associated with each MPR. While a single parameter slightly above the bulk graphite value ($\gtrsim 1.05 \times 10^6$ m.s⁻¹) suffices to fit all MPR for $N \geq 2$ layer systems, We find that v_F increases significantly up to $\approx 1.45 \times 10^6$ m.s⁻¹ in monolayer graphene. This result is understood as a signature of enhanced many-body effects in unscreened graphene.

The low-energy electronic bands and magneto-optical response of mono- and N -layer graphene have been extensively discussed using an effective bilayer model [14, 22–26]. To lowest order, this model uses only two parameters, namely the single-particle Fermi velocity $v_F = 3/2a\gamma_0/\hbar$, where γ_0 is the nearest neighbor hopping parameter, $a = 0.142$ nm is the C–C bond length, and the nearest neighbor interlayer coupling constant γ_1 . The band structure of Bernal- or equivalently AB-stacked $N \geq 2$ layer systems exhibits $2N$ bands, including one pair of linear (monolayer-like) bands only present for odd N and a set of $\lfloor N/2 \rfloor$ effective bilayer bands (here, $\lfloor \cdot \rfloor$ denotes the integer part) with a rescaled $\tilde{\gamma}_1 = 2\gamma_1 \cos \theta$ [23–26], which corresponds to half the energy gap between their split-off bands. The angle θ represent the quantized transverse momenta $\theta = k_z c/2$ at which two-dimensional cuts are made in the three-dimensional electronic dispersion of graphite, with $c/2 = 0.34$ nm the interlayer separation in bulk graphite.

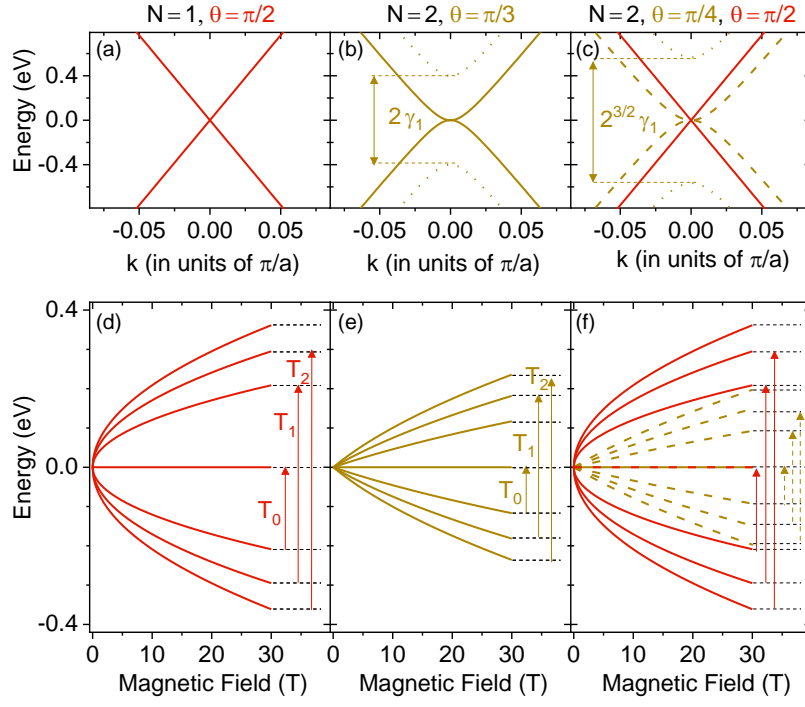


FIG. 1. Single-particle low-energy electronic structure and Landau levels of mono-, bi- and trilayer graphene. The electronic dispersions obtained from the effective bilayer model described in the text are shown in (a-c), respectively. The corresponding dispersion of the Landau levels arising from the gapless bands are shown in (d,e,f) for mono-, bi- and trilayer graphene, respectively. Red lines in (d) and (f) correspond to monolayer-like Landau levels ($\theta = \pi/2$), while dark yellow lines in (e,f) correspond to Landau levels arising from effective bilayers obtained at quantized values of $\theta \neq \pi/2$. The vertical arrows indicate the optically allowed inter LL transitions T_n that give rise to the magneto-phonon resonances. The calculations are performed with $v_F = 1.05 \times 10^6$ m/s and $\gamma_1 = 400$ meV.

The band structure of mono- to trilayer graphene and corresponding values of $\tilde{\gamma}_1$ and θ are shown in Fig. 1a-c.

In the presence of a transverse magnetic field, the ef-

fective mono- and bilayers give rise to independent sets of Landau fans. The energy \mathcal{L}_n^θ ($\mathcal{L}_{-n}^\theta = -\mathcal{L}_n^\theta$) of the n^{th} electron ($n \geq 0$) or hole ($n \leq 0$) LL arising from the gapless bands in an effective bilayer writes [9, 27]:

$$\mathcal{L}_{|n|}^\theta = \sqrt{\frac{\tilde{\gamma}_1^2}{2} + \left(|n| + \frac{1}{2}\right) E_1^2} - \sqrt{\frac{\tilde{\gamma}_1^4}{4} + \left(|n| + \frac{1}{2}\right) E_1^2 \tilde{\gamma}_1^2 + \frac{E_1^4}{4}}, \quad (1)$$

where $E_1 = v_F \sqrt{2e\hbar B}$. At $\theta = \pi/2$, one obtains the well-known LL fan of monolayer graphene $\mathcal{L}_{|n|}^{\pi/2} = \sqrt{n} E_1$. For $\theta \neq \pi/2$, nearly linear scalings of $\mathcal{L}_n^\theta(B)$, characteristic of effective bilayers are observed. The corresponding LL fans are shown in Fig. 1d-f for mono to trilayer graphene, respectively. As previously established [28–30], optically-allowed transitions, such that $\delta|n| = \pm 1$ couple to the graphene G-mode phonons (with energy $\hbar\omega_G \approx 1585$ cm $^{-1}$ or equivalently ≈ 197 meV) and give rise to series of MPR [12, 31, 32], as indicated by the vertical arrows in Fig. 1d-f. In contrast, symmetric inter

LL transitions ($\delta|n| = 0$, denoted L_n , with $n \geq 1$) are Raman-allowed [5, 13, 14] but are not expected to couple to optical phonons [28]. In the following, the energy of the optically-active inter LL transitions associated with a given value of θ will be simply denoted

$$T_n = \left| \mathcal{L}_{\pm n+1}^\theta - \mathcal{L}_{\mp(n)}^\theta \right|, \quad n \geq 0 \quad (2)$$

and the $(n+1)^{\text{th}}$ MPR ($n \geq 0$) occurs when $T_n = \hbar\omega_G$. The suspended graphene samples investigated here were prepared by mechanical cleavage of Bernal stacked

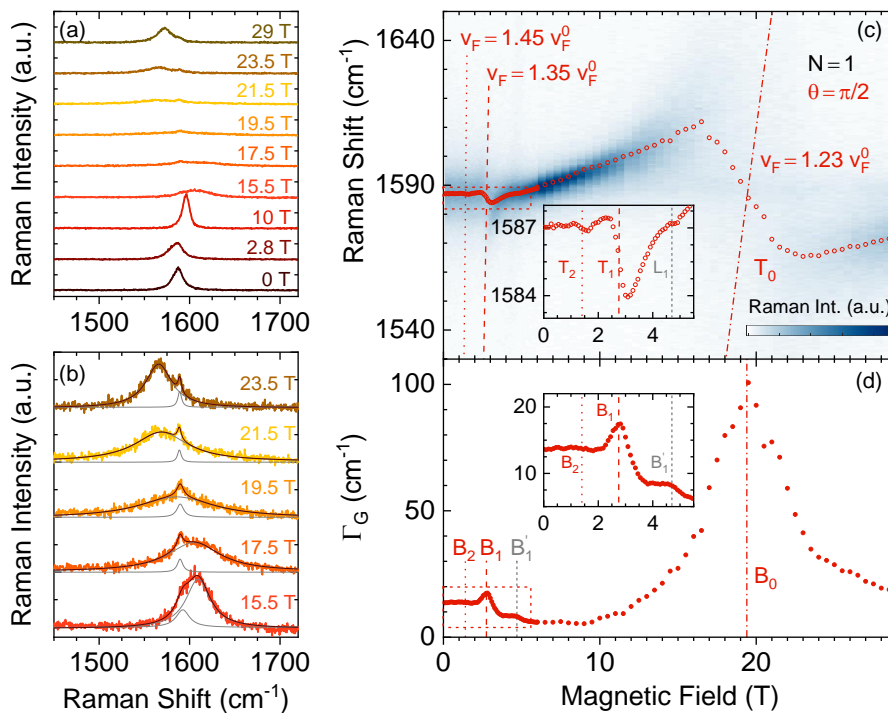


FIG. 2. Magneto-phonon resonances in suspended monolayer graphene. (a,b) Raman G-mode spectra at selected values of the transverse magnetic field B . The spectra are acquired for the same duration and incident laser power and offset for clarity. The dark and light gray lines are Lorentzian fits to the data. (c) G-mode frequency ω_G (red circles), extracted from Lorentzian fits of the G-mode spectra, overlaid on a false-color plot of the Raman spectra as a function of B . The red and grey lines are calculated dispersions of the T_n (optically allowed) and of the L_1 (Raman allowed) transitions, respectively. The velocity parameters (estimated at $\hbar\omega_G$) associated with the three observed MPR are indicated in units of $v_F^0 = 1.00 \times 10^6$ m.s $^{-1}$. (d) Lorentzian full-width at half maximum Γ_G as a function of the magnetic field. The resonant fields B_n are indicated. The insets in (c) and (d) show close-ups on the regions boxed with thin dotted lines.

natural graphite and dry transfer onto 8 μm -diameter pits etched in Si/SiO $_2$ substrates as described in details elsewhere [33, 34]. Such pristine, minimally screened graphene layers have been shown to exhibit negligible residual doping and charge inhomogeneity, making them ideally suited for MMRS studies [5, 14]. The samples were held in a home-built magneto-optical cryostat where MMRS measurements were performed in a back-scattering geometry under transverse magnetic fields up to 29 T. A cw laser beam at 514 nm was focused onto a ~ 2 μm -diameter spot. A cross-circular polarization configuration was implemented, where incoming and Raman scattered photons have opposite helicity. In these conditions, the magneto-Raman spectra are dominated by MPR [28, 35]. We have employed laser powers ~ 1 μW at our samples to minimise laser-induced heating effects while still having a sufficiently large MMRS signal. All measurements were performed at a base temperature of 4 K. Raman G-mode spectra were fit to Lorentzian functions and the peak frequencies and full-width at half maximum are determined with an experimental error that is typically smaller than the symbol size.

Figure 2 shows MMRS data for a suspended graphene

monolayer with minimal native doping (spatially averaged over our laser spot size) well below 10^{12} cm $^{-2}$. MPR appear as anti-crossings involving significant frequency shifts and line broadening of the G-mode feature. Due to electronic broadening in graphene [36, 37], anti-crossings are not fully resolved, particularly so at low field. The third and second MPR, involving transitions T_2 and T_1 appear at $B_2 = 1.45 \pm 0.1$ T and $B_1 = 2.75 \pm 0.1$ T, respectively. Remarkably, for the first time in suspended graphene, we report the $n = 0$ MPR at $B_0 = 19.4 \pm 0.1$ T. The prominence of the T_0 MPR originates from the fact that the coupling strength in MPR theory [32] grows with the LL degeneracy, which is proportional to B . As a result, MPR involving LL with higher n are fainter since these resonances occur at lower B .

The resonant fields observed here are considerably lower than in substrate-supported systems [12, 15, 16] as discussed in more details later. As shown in Fig. 2b, near B_0 , the G-mode exhibits a double-Lorentzian lineshape, with a broad, prominent feature that shows an avoided crossing with the T_0 transition and a fainter sub-feature (not displayed in Fig. 2c,d) that is virtually independent on B . The integrated intensity of this *uncoupled* sub-

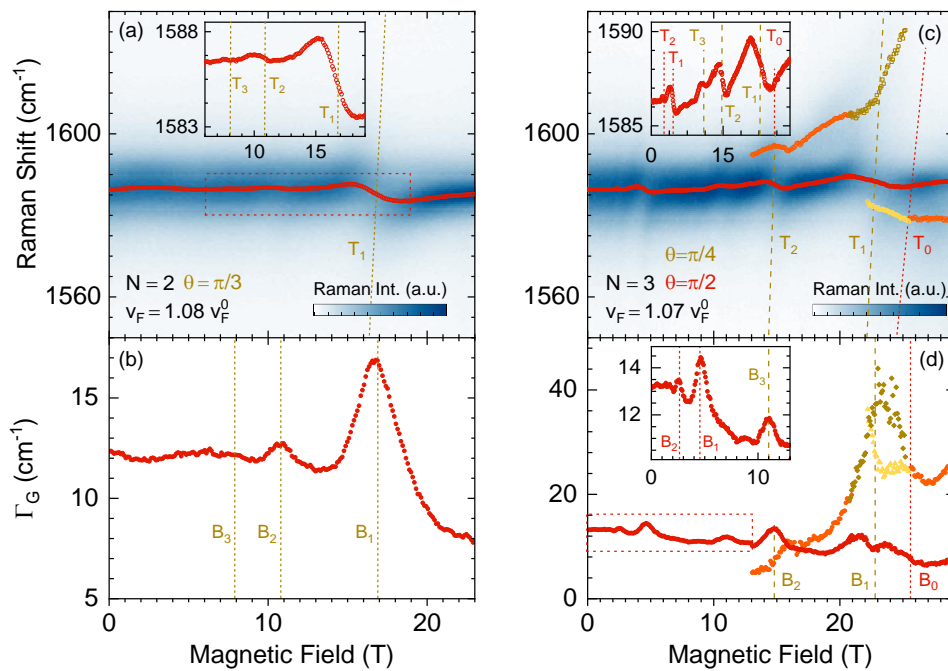


FIG. 3. Magneto-phonon resonances in suspended bi- (a,b) and trilayer (c,d) graphene. (a,c) G-mode frequency ω_G (red circles), extracted from a Lorentzian fit of the G-mode spectra, overlaid on a false-color plot of the Raman spectra as a function of the transverse magnetic field B . The red and dark yellow dashed lines are calculated dispersions of the T_n transitions for monolayer-like and effective bilayer bands. The single v_F extracted from all MPR is indicated in both cases in units of $v_F^0 = 1.00 \times 10^6 \text{ m.s}^{-1}$. (b,d) Lorentzian full-width at half maximum Γ_G as a function of the magnetic field. The resonant fields B_n are indicated with color-coded values of θ . In the trilayer case (c, d), the G-mode spectra are fit to a double Lorentzian (red and orange symbols) for $13 \text{ T} < B < 21 \text{ T}$ and to a triple Lorentzian (red, yellow and dark yellow) for $21 \text{ T} < B < 26 \text{ T}$ near the first monolayer-like and second bilayer-like MPR. The insets in (a,b,d) show close-ups on the regions boxed with red dotted lines in (a,d) and on the most prominent G-mode sub-feature in (c).

feature is about one order of magnitude smaller than that of the coupled G-mode feature (Fig. 2b); its frequency at $1589.2 \pm 0.8 \text{ cm}^{-1}$ is slightly upshifted and its full-width at half maximum ($6.5 \pm 1.5 \text{ cm}^{-1}$) is significantly lower as compared with the G-mode feature recorded at $B = 0 \text{ T}$ ($\omega_G = 1587.0 \pm 0.1 \text{ cm}^{-1}$, $\Gamma_G = 13.6 \pm 0.1 \text{ cm}^{-1}$). These characteristics suggest a slight doping with a Fermi level slightly above $\hbar\omega_G/2$ (i.e., $\sim 100 \text{ meV}$) [38–40]. We therefore suggest that local inhomogeneities at the nanometer scale may result in an uncoupled G-mode sub-feature due to Pauli blocking of the T_0 transition [15, 41]. Importantly, Ref. 15 reported a similar uncoupled G-mode feature in SiO_2 -supported graphene, however with a large integrated intensity, comparable with that of the coupled G-mode feature that follows an anti-crossing with the T_0 transition. Here, the much lower spectral weight of the uncoupled G-mode sub-feature illustrates the superior spatial homogeneity of suspended graphene. We suggest that MMRS near the $n = 0$ MPR can be used as a quantitative probe of residual electron and hole puddles in high-quality graphene.

In Fig. 2c, one can clearly see an increase of the phonon linewidth, a signature of a variation of the phonon life-

time induced by an interaction, at $B'_1 = 4.7 \pm 0.1 \text{ T}$. This resonance implies the G-mode phonon and the symmetric inter LL excitation L_1 . Although symmetric electronic excitations should not couple to the optical phonons [28], a similar MPR has been observed in graphene on graphite [13] and on graphene encapsulated in hexagonal Boron Nitride (BN) [16]. Interestingly, both in suspended graphene and in BN-encapsulated graphene, these nominally forbidden MPR are much fainter than the allowed MPR involving T_1 and have similar strength. Here, since we investigate suspended graphene, substrate-induced effects cannot account for this unexpected coupling. Our results point towards an intrinsic effect, possibly originating from LL mixing induced by Coulomb interactions [42].

We now consider how MPR evolve for thicker graphene stacks, as the electronic structure gets increasingly complex. Figure 3 shows MPR data for suspended bilayer and trilayer graphene. Data for tetra- and penta-layer graphene are reported in Fig. 4. These data were acquired using a lower spectral resolution than for $N = 1, 2, 3$. As a result, we have not attempted to resolve signatures of pronounced anti-crossings at high fields for

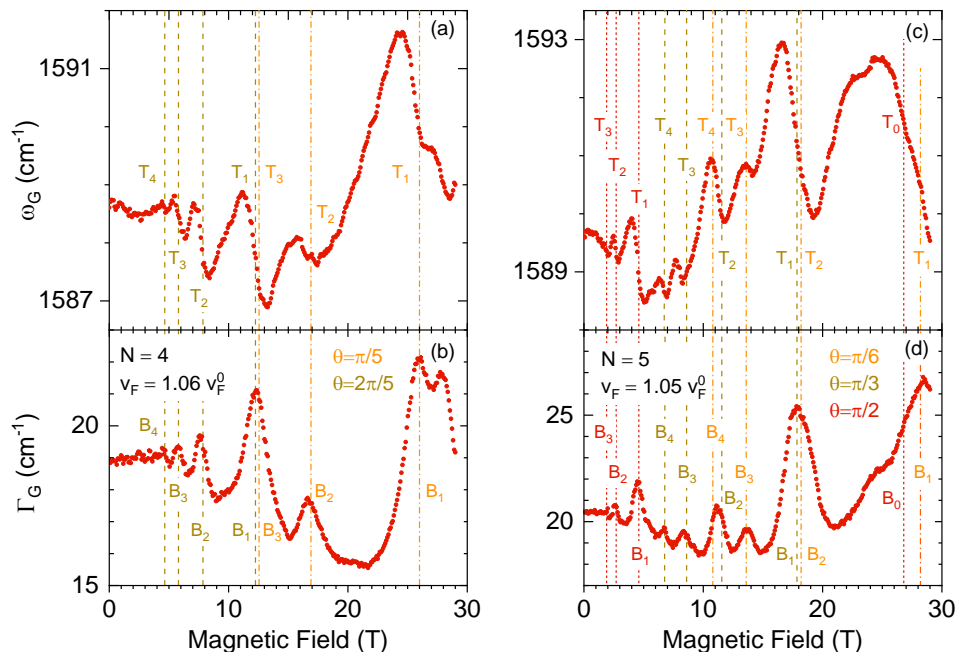


FIG. 4. Magneto-phonon resonances in suspended tetra- (a,b) and pentalayer (c,d) graphene. (a,c) G-mode frequency ω_G (red circles), extracted from a Lorentzian fit of the G-mode spectra as a function of the transverse magnetic field B . The red, dark yellow and orange dashed lines are calculated dispersions of the T_n transitions for monolayer-like and effective bilayer bands with color-coded values of θ . The single v_F extracted from all MPR is indicated in both cases in units of $v_F^0 = 1.00 \times 10^6 \text{ m.s}^{-1}$. (b,d) Lorentzian full-width at half maximum Γ_G as a function of the magnetic field. The resonant fields B_n are indicated with color-coded values of θ .

$N = 4$ and $N = 5$. For $N = 2$, three MPR are resolved at $B_3 = 7.9 \pm 0.1 \text{ T}$, $B_2 = 10.8 \pm 0.1 \text{ T}$, $B_1 = 16.6 \pm 0.1 \text{ T}$ and are assigned to the T_3 , T_2 and T_1 MPR of bilayer graphene ($\theta = \pi/3$), respectively. In trilayer graphene (Fig. 3c,d), we are able to resolve the first three monolayer-like MPR (involving transitions T_0 , T_1 , T_2 for $\theta = \pi/2$) and the MPR associated with T_1 , T_2 , T_3 for the effective bilayer ($\theta = \pi/4$). At high fields $B > 14 \text{ T}$, the G-mode lineshape becomes more complex due to the overlap between the second bilayer-like MPR (T_1 , $\theta = \pi/4$) and first monolayer-like MPR (T_0 , $\theta = \pi/2$). These spectra are well fit to a bilayer Lorentzian form for $13 \text{ T} < B < 21 \text{ T}$ and $26 \text{ T} < B < 29 \text{ T}$ and to a triple Lorentzian (red, yellow and dark yellow) for $21 \text{ T} < B < 26 \text{ T}$. The narrow, central feature (red symbols in Fig. 3c) is assigned to the second bilayer-like MPR (T_1 , $\theta = \pi/4$), while the broader and shifted features (orange symbols for double-Lorentzian fits then dark yellow and yellow symbols for triple-Lorentzian fits in Fig. 3c) are assigned to the first monolayer-like MPR (T_0 , $\theta = \pi/2$).

In tetralayer graphene (Fig. 4a,b), under transverse magnetic fields up to $B = 29 \text{ T}$, we observe six MPR associated with gapless effective bilayer bands at $\theta = \pi/5$ and $\theta = 2\pi/5$, respectively [43]. Up to nine MPR are observed in the same window for pentalayer graphene (Fig. 4c,d). These MPR are associated with the effective

monolayer ($\theta = \pi/2$), with two other subsets of MPR stemming from the gapless effective bilayer bands at $\theta = \pi/3$ and $\theta = \pi/6$, respectively. Let us note that as the number of electronic subbands increase, MPR involving distinct values of θ and n may be nearly degenerate. As a result, we are not able to clearly resolve T_1 , $\theta = 2\pi/5$ and T_3 , $\theta = \pi/5$ near 12 T for $N = 4$ (Fig. 4c,d). Similarly, for $N = 5$ (Fig. 4c,d), the MPR associated with T_2 , $\theta = \pi/3$ and T_4 , $\theta = \pi/6$ near 11 T as well as with T_0 , $\theta = \pi/2$ and T_1 , $\theta = \pi/6$ near 27-28 T appear as single, slightly broadened MPR. Thus, the growing complexity of the LL spectrum with increasing N prevents detailed studies of MPR for $N > 5$, until the limit of the LL fan diagram of bulk graphite is reached.

As shown in Fig. 5a, from the data in Fig. 2-4 and using the effective bilayer model (Eq. (2)), we can now determine, for each MPR, the velocity parameters $v_{F,n}$ evaluated at resonant fields B_n . For simplicity, we have considered a constant $\gamma_1 = 400 \text{ meV}$ for all N and have attempted a global fit of all the B_n measured for a given N . For $N = 2$ to $N = 5$, This procedure yields a very good agreement between Eq. (2) and our experiments with a constant v_F that decreases smoothly from $(1.08 \pm 0.01) \times 10^6 \text{ m.s}^{-1}$ for $N = 2$ down to $(1.05 \pm 0.01) \times 10^6 \text{ m.s}^{-1}$ for $N = 5$. These values converge towards the bulk graphite value of $(1.02 \pm 0.01) \times 10^6 \text{ m.s}^{-1}$ [25] and are in excellent agreement with previous electronic

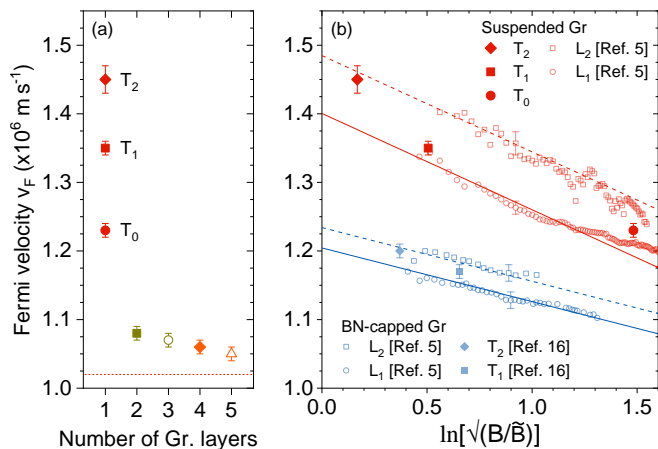


FIG. 5. (a) Velocity parameters v_F extracted from the magneto-phonon resonances in Fig. 2-4 as a function of N , the number of graphene layers. (b) Velocity parameters in suspended monolayer graphene (filled red symbols) as a function of $\ln \sqrt{B/\tilde{B}}$, with $\tilde{B} = 1$ T. These velocity parameters are compared with those obtained from electronic Raman scattering measurements reproduced from Ref. 5), with the symmetric L_1 and L_2 transitions in the same sample (open red symbols) and in a graphene sample encapsulated in hexagonal boron nitride (BN, open blue symbols). The solid and dashed lines are theoretical calculations reproduced from Ref. 5. These calculations include electron-electron interactions (i.e., the electron self-energy) and magneto-excitonic effects. For comparison, we show (blue symbols) the values of v_F measured in Ref. 16 in BN-capped graphene.

Raman measurements on the same samples [14].

In contrast, a single velocity parameter would grossly fail to fit the three observed MPR (involving T_n , with $n = 0, 1, 2$) in monolayer graphene. Instead, using Eq. (2), we determine that v_F increases significantly from $v_{F,0} = (1.23 \pm 0.01) \times 10^6$ m.s $^{-1}$ up to $v_{F,2} = (1.45 \pm 0.02) \times 10^6$ m.s $^{-1}$ as B_n decreases from 19.4 T down to 1.40 T. Interestingly, our value of $v_{F,1} = (1.35 \pm 0.1) \times 10^6$ m.s $^{-1}$ inferred from the $n = 1$ MPR exactly matches a recent report in neutral suspended graphene grown by chemical vapor deposition and carefully cleaned after transfer (Ref. 18).

The rise of $v_{F,n}$ as B_n decreases is qualitatively consistent with our previous measurements [5] and may arise from the combination of two effects: i) a logarithmic divergence of v_F as B_n decreases (self-energy) and ii) magneto-Coulomb binding, leading n -dependent v_F associated with T_n or L_n transitions. We should stress that MPR probe charge carriers at a fixed energy set by $\hbar\omega_G = T_n$. However, in a one-electron picture, MPR occur at $B_n \propto (\sqrt{n+1} + \sqrt{n})^{-1}$ for $N = 1$ (Eq. (2)). Previous investigations of L_n transitions, in suspended graphene (Ref. 5) and of T_n transitions in BN-encapsulated graphene (Ref. 20) indicate that at a

given B , v_F increases with n , up to $n = 3$ (see also Fig. 5b). Our data are in line with these results, since $v_{F,0} < v_{F,1} < v_{F,2}$ (Fig. 2c). However, Ref. 20 also reports a slight decrease of v_F at fixed B for higher order T_n (with $n = 3, 4, 5$). In the wake of recent studies of filling-factor dependent many-body effects in graphene [18, 20, 44, 45], further efforts are needed to separate the contributions of self-energy and magneto-Coulomb binding to the renormalization of v_F .

Remarkably, in keeping with our previous measurements of L_n transitions [14], many-body effects are essentially observed in monolayer graphene and nearly vanish for $N \geq 2$. Such observations are consistent with recent works showing that the reduction of the exciton binding energy in an atomically thin semiconductor coupled to graphene layers is readily maximized with one graphene monolayer and does not increase further if a bilayer graphene is used instead [46]. In addition, the parabolic dispersion of massive fermions in effective bilayers (Fig. 1b,c) creates a finite density of states at the Dirac point, which may be sufficient to quench electron-electron interactions and the subsequent renormalization of electronic bands. Here also, additional investigations of many-body effects are required to account for the abrupt transition between the mono and bilayer cases [47, 48].

In conclusion, we have demonstrated that magneto-phonon resonances provide invaluable fingerprints of the low-energy electronic dispersion of suspended graphene layers, which are in excellent quantitative agreement with a one-electron effective bilayer model for $N \geq 2$. In the monolayer limit, electrons undergo minimal screening, leading to pronounced many-body effects which, to experimental accuracy, do not yield sizeable experimental signatures for $N \geq 2$. Many-body effects in graphene and Dirac fermions in general continue to attract considerable interest and future directions include the interplay between of many-body effects and electronic lifetime in graphene and related systems [49].

Acknowledgements

We are grateful to D.M. Basko for fruitful discussions. We thank I. Breslavetz, the StNano clean room staff, M. Romeo, F. Chevrier, A. Boulard and the IPCMS workshop for technical support. We acknowledge financial support from the Agence Nationale de Recherche (ANR) under grants H2DH ANR-15-CE24-0016, ANR-17-CE24-0030, 2D-POEM ANR-18-ERC1-0009, the Labex NIE project ANR-11-LABX-0058-NIE and the USIAS GOLEM project, within the Investissement d'Avenir program ANR-10-IDEX-0002-02. M.P. and C.F. acknowledge support from the EC Graphene Flagship project (no. 604391). Part of this work was performed at the LNCMI-Grenoble, a member of the European Magnetic Field Laboratory (EMFL).

* stephane.berciaud@ipcms.unistra.fr

† clement.faugeras@lncmi.cnrs.fr

- [1] K. I. Bolotin, K. J. Sikes, Z. Jiang, M. Klima, G. Fudenberg, J. Hone, P. Kim, and H. L. Stormer, "Ultra-high electron mobility in suspended graphene," *Solid State Commun.* **146**, 351–355 (2008).
- [2] X. Du, I. Skachko, A. Barker, and E. Y. Andrei, "Approaching ballistic transport in suspended graphene," *Nat Nano* **3**, 491–495 (2008).
- [3] K. I. Bolotin, F. Ghahari, M. D. Shulman, H. L. Stormer, and P. Kim, "Observation of the fractional quantum hall effect in graphene," *Nature* **462**, 196–199 (2009).
- [4] D. C. Elias, R. V. Gorbachev, A. S. Mayorov, S. V. Morozov, A. A. Zhukov, P. Blake, L. A. Ponomarenko, I. V. Grigorieva, K. S. Novoselov, F. Guinea, and A. K. Geim, "Dirac cones reshaped by interaction effects in suspended graphene," *Nature Physics* **7**, 701–704 (2011).
- [5] C. Faugeras, S. Berciaud, P. Leszczynski, Y. Henni, K. Nogajewski, M. Orlita, T. Taniguchi, K. Watanabe, C. Forsythe, P. Kim, R. Jalil, A.K. Geim, D.M. Basko, and M. Potemski, "Landau level spectroscopy of electron-electron interactions in graphene," *Phys. Rev. Lett.* **114**, 126804 (2015).
- [6] K. F. Mak, L. Ju, F. Wang, and T. F. Heinz, "Optical spectroscopy of graphene: From the far infrared to the ultraviolet," *Exploring Graphene, Recent Research Advances*, *Solid State Commun.* **152**, 1341–1349 (2012).
- [7] A. Castellanos-Gomez, V. Singh, H. S. J. van der Zant, and G. A. Steele, "Mechanics of freely-suspended ultrathin layered materials," *Annalen der Physik* **527**, 27–44 (2015).
- [8] D. N. Basov, M. M. Fogler, A. Lanzara, Feng Wang, and Yuanbo Zhang, "*Colloquium* : Graphene spectroscopy," *Rev. Mod. Phys.* **86**, 959–994 (2014).
- [9] M. Orlita and M. Potemski, "Dirac electronic states in graphene systems: Optical spectroscopy studies," *Semicond. Sci. Technol.* **25**, 063001 (2010).
- [10] G. Li, A. Luican, and E. Y. Andrei, "Scanning tunneling spectroscopy of graphene on graphite," *Phys. Rev. Lett.* **102**, 176804 (2009).
- [11] Zhi-Guo Chen, Zhiwen Shi, Wei Yang, Xiaobo Lu, You Lai, Hugen Yan, Feng Wang, Guangyu Zhang, and Zhiqiang Li, "Observation of an intrinsic bandgap and Landau level renormalization in graphene/boron-nitride heterostructures," *Nature communications* **5**, 4461 (2014).
- [12] C. Faugeras, M. Amado, P. Kossacki, M. Orlita, M. Sprinkle, C. Berger, W. A. de Heer, and M. Potemski, "Tuning the electron-phonon coupling in multilayer graphene with magnetic fields," *Phys. Rev. Lett.* **103**, 186803 (2009).
- [13] C. Faugeras, M. Amado, P. Kossacki, M. Orlita, M. Kühne, A. A. L. Nicolet, Yu. I. Latyshev, and M. Potemski, "Magneto-Raman scattering of graphene on graphite: Electronic and phonon excitations," *Phys. Rev. Lett.* **107**, 036807 (2011).
- [14] S. Berciaud, M. Potemski, and C. Faugeras, "Probing electronic excitations in mono- to pentalayer graphene by micro magneto-raman spectroscopy," *Nano Lett.* **14**, 4548–4553 (2014).
- [15] Y. Kim, J. M. Poumirol, A. Lombardo, N. G. Kalugin, T. Georgiou, Y. J. Kim, K. S. Novoselov, A. C. Ferrari, J. Kono, O. Kashuba, V. I. Fal'ko, and D. Smirnov, "Measurement of filling-factor-dependent magnetophonon resonances in graphene using Raman spectroscopy," *Phys. Rev. Lett.* **110**, 227402 (2013).
- [16] C. Neumann, S. Reichardt, M. Drögeler, B. Terrés, K. Watanabe, T. Taniguchi, B. Beschoten, S. V. Rotkin, and C. Stampfer, "Low B field magneto-phonon resonances in single-layer and bilayer graphene," *Nano Lett.* **15**, 1547–1552 (2015).
- [17] T. Kazimierzczuk, A. Bogucki, T. Smoleński, M. Goryca, C. Faugeras, P. Machnikowski, M. Potemski, and P. Kosacki, "Time-resolved magneto-Raman study of carrier dynamics in low Landau levels of graphene," *Phys. Rev. B* **100**, 075401 (2019).
- [18] J. Sonntag, S. Reichardt, L. Wirtz, B. Beschoten, M. I. Katsnelson, F. Libisch, and C. Stampfer, "Impact of many-body effects on Landau levels in graphene," *Phys. Rev. Lett.* **120**, 187701 (2018).
- [19] E. Riccardi, M.-A. Méasson, M. Cazayous, A. Sacuto, and Y. Gallais, "Gate-dependent electronic Raman scattering in graphene," *Phys. Rev. Lett.* **116**, 066805 (2016).
- [20] B. Jordan Russell, Boyi Zhou, T. Taniguchi, K. Watanabe, and Erik A. Henriksen, "Many-particle effects in the cyclotron resonance of encapsulated monolayer graphene," *Phys. Rev. Lett.* **120**, 047401 (2018).
- [21] A. C. Ferrari and D. M. Basko, "Raman spectroscopy as a versatile tool for studying the properties of graphene," *Nature Nano* **8**, 235–246 (2013).
- [22] S. Latil and L. Henrard, "Charge carriers in few-layer graphene films," *Physical Review Letters* **97**, 036803 (2006).
- [23] M. Koshino and T. Ando, "Orbital diamagnetism in multilayer graphenes: Systematic study with the effective mass approximation," *Phys. Rev. B* **76**, 085425 (2007).
- [24] B. Partoens and F. M. Peeters, *Phys. Rev. B* **75**, 193402 (2007).
- [25] M. Orlita, C. Faugeras, J. M. Schneider, G. Martinez, D. K. Maude, and M. Potemski, "Graphite from the viewpoint of Landau level spectroscopy: An effective graphene bilayer and monolayer," *Phys. Rev. Lett.* **102**, 166401 (2009).
- [26] Kin Fai Mak, Matthew Y. Sfeir, James A. Misewich, and Tony F. Heinz, "The evolution of electronic structure in few-layer graphene revealed by optical spectroscopy," *Proceedings of the National Academy of Sciences* **107**, 14999 (2010).
- [27] E. McCann and V. I. Fal'ko, "Landau-level degeneracy and quantum Hall effect in a graphite bilayer," *Phys. Rev. Lett.* **96**, 086805 (2006).
- [28] O. Kashuba and V. I. Fal'ko, "Signature of electronic excitations in the Raman spectrum of graphene," *Phys. Rev. B* **80**, 241404 (2009).
- [29] Marcin Mucha-Kruczyński, Oleksiy Kashuba, and Vladimir I. Fal'ko, "Spectral features due to inter-Landau-level transitions in the Raman spectrum of bilayer graphene," *Phys. Rev. B* **82**, 045405 (2010).
- [30] P. Kossacki, C. Faugeras, M. Kühne, M. Orlita, A. A. L. Nicolet, J. M. Schneider, D. M. Basko, Yu. I. Latyshev, and M. Potemski, "Electronic excitations and electron-phonon coupling in bulk graphite through Raman scattering in high magnetic fields," *Phys. Rev. B* **84**, 235138 (2011).

- [31] T. Ando, “Magnetic oscillation of optical phonon in graphene,” *J. Phys. Soc. Jpn.* **76**, 024712 (2007).
- [32] M. O. Goerbig, J.-N. Fuchs, K. Kechedzhi, and V. I. Fal’ko, “Filling-factor-dependent magnetophonon resonance in graphene,” *Phys. Rev. Lett.* **99**, 087402 (2007), erratum: *ibid.* **103** (17): 179901, 2009.
- [33] S. Berciaud, S. Ryu, L. E. Brus, and T. F. Heinz, “Probing the intrinsic properties of exfoliated graphene: Raman spectroscopy of free-standing monolayers,” *Nano Lett.* **9**, 346–352 (2009).
- [34] D. Metten, F. Federspiel, M. Romeo, and S. Berciaud, “All-optical blister test of suspended graphene using micro-raman spectroscopy,” *Phys. Rev. Applied* **2**, 054008 (2014).
- [35] M. Kühne, C. Faugeras, P. Kossacki, A. A. L. Nicolet, M. Orlita, Yu. I. Latyshev, and M. Potemski, “Polarization-resolved magneto-raman scattering of graphenelike domains on natural graphite,” *Phys. Rev. B* **85**, 195406 (2012).
- [36] Aaron Bostwick, Taisuke Ohta, Thomas Seyller, Karsten Horn, and Eli Rotenberg, “Quasiparticle dynamics in graphene,” *Nature Physics* **3**, 36–40 (2007).
- [37] Christoph Neumann, Donatus Halpaap, Sven Reichardt, Luca Banszerus, Michael Schmitz, Kenji Watanabe, Takashi Taniguchi, Bernd Beschoten, and Christoph Stampfer, “Probing electronic lifetimes and phonon anharmonicities in high-quality chemical vapor deposited graphene by magneto-raman spectroscopy,” *Applied Physics Letters* **107**, 233105 (2015).
- [38] S. Pisana, M. Lazzeri, C. Casiraghi, K. Novoselov, A. Geim, A. Ferrari, and F. Mauri, “Breakdown of the adiabatic Born-Oppenheimer approximation in graphene,” *Nat. Mater.* **6**, 198–201 (2007).
- [39] J. Yan, Y. Zhang, P. Kim, and A. Pinczuk, “Electric field effect tuning of electron-phonon coupling in graphene,” *Phys. Rev. Lett.* **98**, 166802 (2007).
- [40] Guillaume Froehlicher and Stéphane Berciaud, “Raman spectroscopy of electrochemically gated graphene transistors: Geometrical capacitance, electron-phonon, electron-electron, and electron-defect scattering,” *Phys. Rev. B* **91**, 205413 (2015).
- [41] Przemyslaw Leszczynski, Zheng Han, Aurelien A. L. Nicolet, Benjamin A. Piot, Piotr Kossacki, Milan Orlita, Vincent Bouchiat, Denis M. Basko, Marek Potemski, and Clement Faugeras, “Electrical switch to the resonant magneto-phonon effect in graphene,” *Nano Letters* **14**, 1460–1466 (2014).
- [42] R. Roldán, J.-N. Fuchs, and M. O. Goerbig, “Spin-flip excitations, spin waves, and magnetoexcitons in graphene landau levels at integer filling factors,” *Phys. Rev. B* **82**, 205418 (2010).
- [43] C. Faugeras, P. Kossacki, A.A.L. Nicolet, M. Orlita, M. Potemski, and D.M. Basko, “Probing the band structure of quadri-layer graphene with magneto-phonon resonance,” *New J. of Phys.* **14**, 095007 (2012).
- [44] Alexey A. Sokolik and Yurii E. Lozovik, “Many-body filling factor dependent renormalization of fermi velocity in graphene in strong magnetic field,” *Phys. Rev. B* **99**, 085423 (2019).
- [45] K. Shizuya, “Many-body effects on landau-level spectra and cyclotron resonance in graphene,” *Phys. Rev. B* **98**, 115419 (2018).
- [46] Etienne Lorchat, Luis E. Parra Lopez, Cdric Robert, Delphine Lagarde, Guillaume Froehlicher, Takashi Taniguchi, Kenji Watanabe, Xavier Marie, and Stéphane Berciaud, “Filtering the photoluminescence spectra of atomically thin semiconductors with graphene,” *Nature Nanotechnology* **15**, 283 (2020).
- [47] K. Shizuya, “Many-body corrections to cyclotron resonance in monolayer and bilayer graphene,” *Phys. Rev. B* **81**, 075407 (2010).
- [48] K. Shizuya, “Renormalization and cyclotron resonance in bilayer graphene with weak electron-hole asymmetry,” *Phys. Rev. B* **84**, 075409 (2011).
- [49] Ho-Kin Tang, J. N. Leaw, J. N. B. Rodrigues, I. F. Herbut, P. Sengupta, F. F. Assaad, and S. Adam, “The role of electron-electron interactions in two-dimensional dirac fermions,” *Science* **361**, 570–574 (2018).